## Supplementary Information

# In-situ epitaxial growth and electrochemical conversion of $LiNi_{0.5}Mn_{1.5}O_4$ thin layer on Ni-rich cathode materials for high voltage lithium-ion batteries

Cong Li [a,b], Chun Liu [a], Honglei Liu [a], Chengzhi Hu [a], Yong Wu [a], Afei Li [a], Zhangxian Chen [a,b], Zeheng Yang [a*], Weixin Zhang [a,b*]

[a] *School of Chemistry and Chemical Engineering, Hefei University of Technology and Anhui Key Laboratory of Controllable Chemical Reaction & Material Chemical Engineering, Hefei, Anhui, 230009, China*

[b] *Institute of Energy, Hefei Comprehensive National Science Center, Hefei, Anhui, 230031, China*

* Corresponding authors

E-mails: Zeheng Yang, zehengyang@hfut.edu.cn; Weixin Zhang, wxzhang@hfut.edu.cn

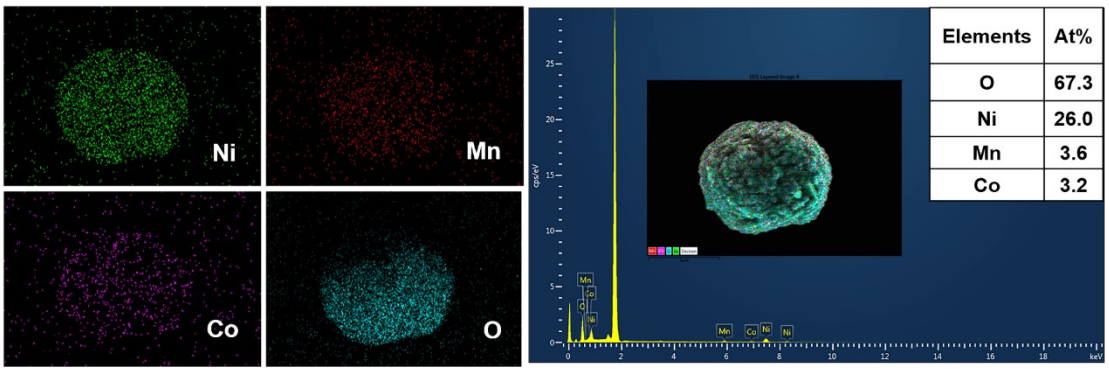


**Figure S1.** Elemental mappings and EDS spectrum of the $Ni_{0.8}Co_{0.1}Mn_{0.1}(OH)_2$ precursor.

The EDS spectrum of $Ni_{0.8}Co_{0.1}Mn_{0.1}(OH)_2$ gives Ni, Co and Mn atomic ratios of 8.125, 1 and 1.125, respectively, which are very close to their target values.

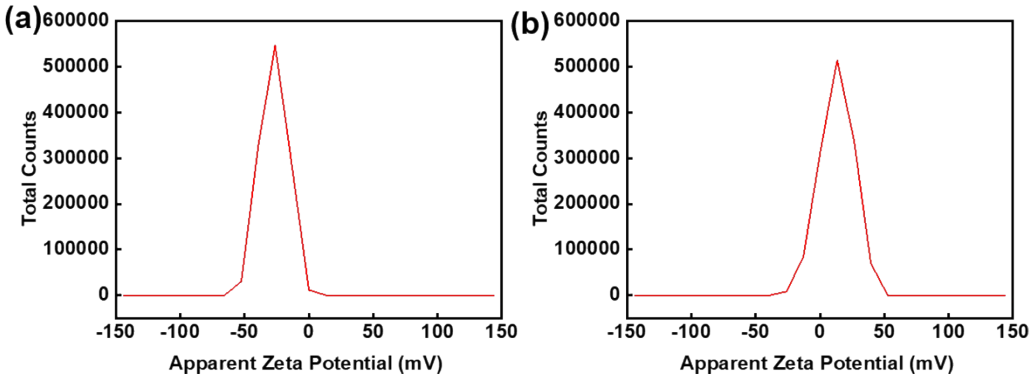


**Figure S2.** Zeta Potential of (a) $Ni_{0.8}Co_{0.1}Mn_{0.1}(OH)_2$ and (b) $Ni(COOCH_3)_2{\cdot}4H_2O$ and $Mn(COOCH_3)_2{\cdot}4H_2O$ in ethanol.

When $Ni(COOCH_3)_2{\cdot}4H_2O$ and $Mn(COOCH_3)_2{\cdot}4H_2O$ is dissolved in ethanol, it is observed that the solution is electropositive. However, when $Ni_{0.8}Co_{0.1}Mn_{0.1}(OH)_2$ is dispersed in ethanol, it is observed that the solution is electronegative. The $Ni^{2+}$ and $Mn^{2+}$ ions are able to be adsorbed on the surface of NCM811 precursors with the electronegaitivity.

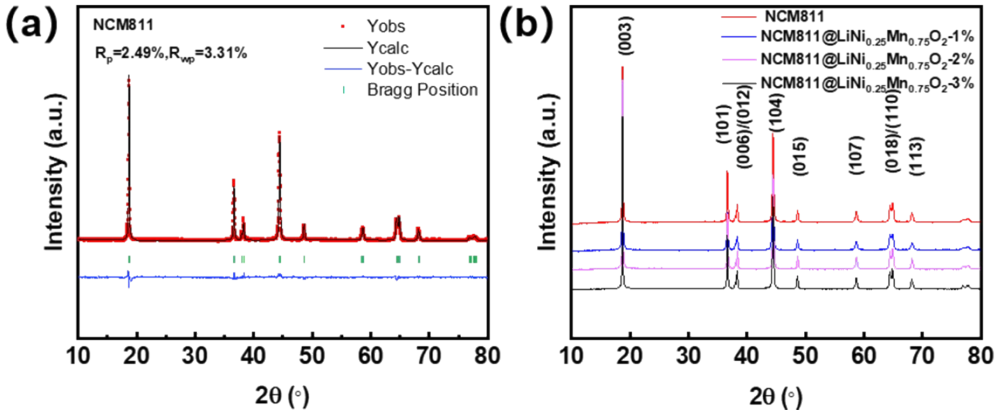


**Figure S3.** Rietveld refinement results of (a) NCM811 sample. (b) XRD patterns of NCM811, NCM811@$LiNi_{0.25}Mn_{0.75}O_2$-1%, NCM811@$LiNi_{0.25}Mn_{0.75}O_2$-2% and NCM811@$LiNi_{0.25}Mn_{0.75}O_2$-3% samples.

Rietveld refinement of XRD results for NCM811 and XRD patterns of other $LiNi_{0.25}Mn_{0.75}O_2$ coating samples are listed in Figure S3. The XRD pattern of NCM811 material can be indexed to layered-$NaFeO_2$ structure, the *R-3m* space group. Rietveld refinement of the XRD results indicates that the introduction of the $LiNi_{0.25}Mn_{0.75}O_2$ coating layer doesn't significantly change the crystallographic parameters (Table S2). The splitting of (006) / (012) planes and (108) / (110) planes indicate that the material is well crystallized with a good layered structure, and all the planes are consistent with the characteristics of hexagonal crystal structure.

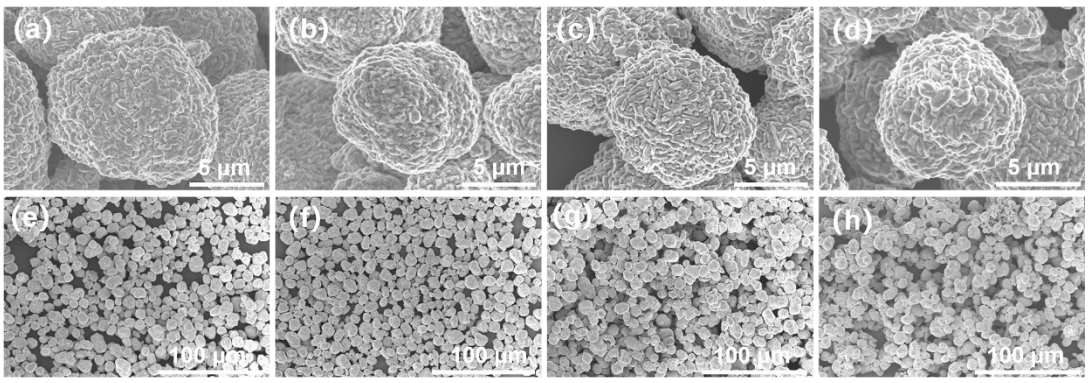


**Figure S4.** FESEM images of (a, e) NCM811, (b, f) NCM811@$LiNi_{0.25}Mn_{0.75}O_2$-1%, (c, g) NCM811@$LiNi_{0.25}Mn_{0.75}O_2$-2%, (d, h) NCM811@$LiNi_{0.25}Mn_{0.75}O_2$-3% samples.

The pristine NCM811 sample exist in micron-sized spherical particles composed of nano-sized primary crystals. After epitaxial coating of $LiNi_{0.25}Mn_{0.75}O_2$, the modified NCM811 samples also maintain the spherical secondary particles.

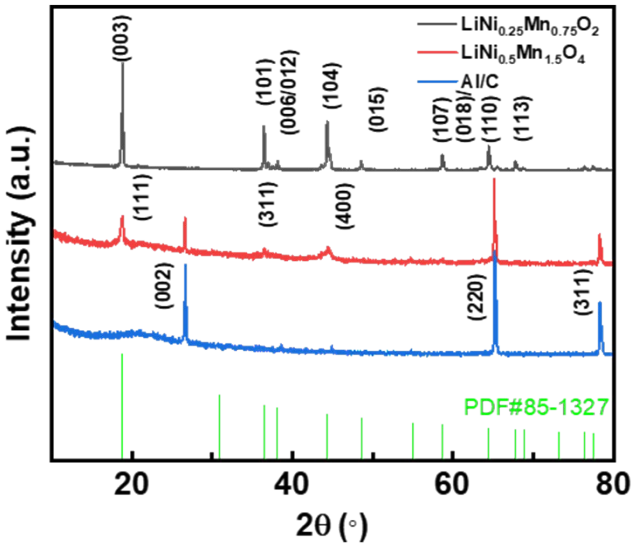


**Figure S5.** XRD patterns of the $LiNi_{0.25}Mn_{0.75}O_2$、 $LiNi_{0.5}Mn_{1.5}O_4$ and current collector Al/C.

The NCM811@$LiNi_{0.25}Mn_{0.75}O_2$-1% electrode is assembled into coin cell. After one cycle of charge and discharge, we can determine the transformation of $LiNi_{0.25}Mn_{0.75}O_2$ into $LiNi_{0.5}Mn_{1.5}O_4$ by XRD measurements. From Figure S5, it can be seen that the (111), (311) and (400) planes correspond to the planes of $LiNi_{0.5}Mn_{1.5}O_4$ (PDF#85-1327). The (002) plane ascribes to the carbon, and (220) and (311) correspond to the planes of Al from the current collector, respectively.

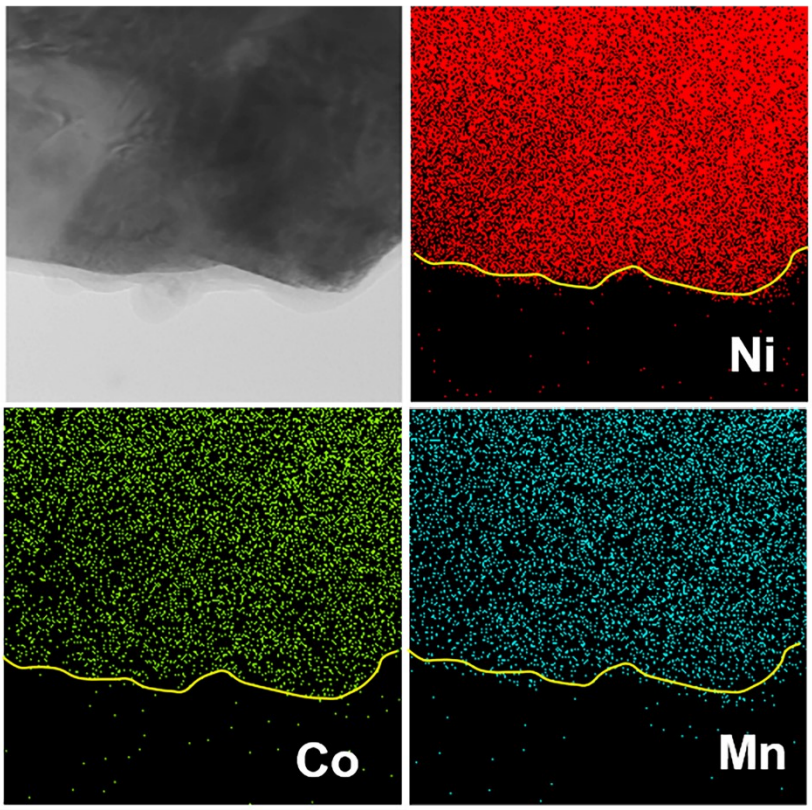


**Figure S6.** Elemental mappings of Ni, Co and Mn in NCM811@LNM-1%.

Ni, Co and Mn elemental mappings of the NCM811@LNM-1% sample are shown in Figure S6. It can be seen that Ni and Mn elements are homogeneously distributed in the particle, while Co element is less distributed in the outer layer of the particle, consistent with the characteristics of the LNM coating layer.

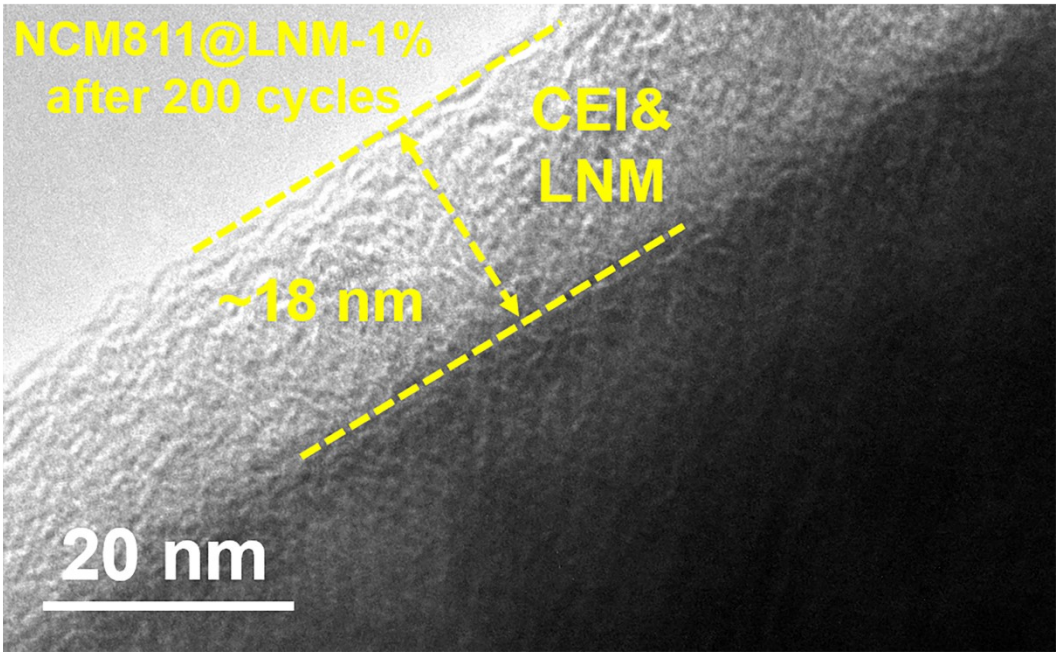


**Figure S7.** HRTEM image of NCM811@LNM-1% after 200 cycles.

As shown in Figure S7, the NCM811@LNM-1% displays a uniform LNM and CEI mixed layer of about 18 nm in thickness on the surface after 200 cycles.

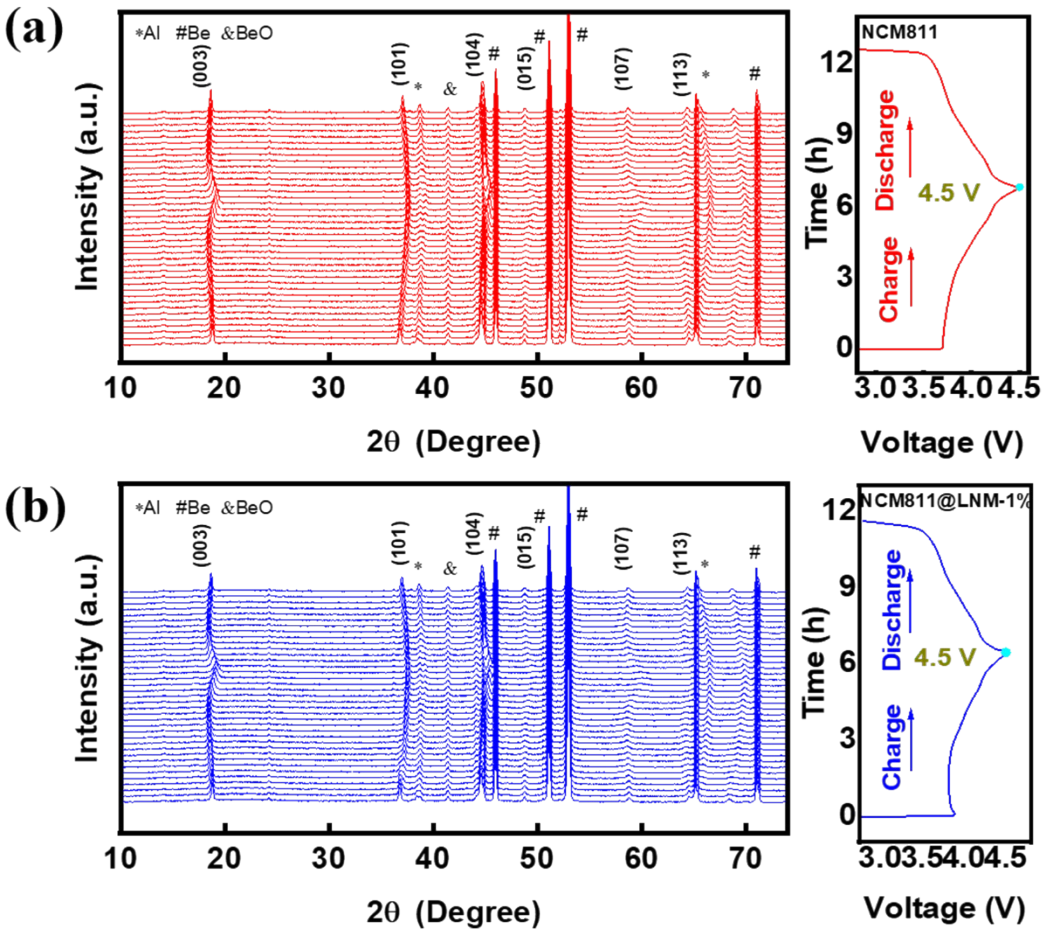


**Figure S8.** Operando XRD characterization for (a) NCM811 and (b) NCM811@LNM-1% cathodes during the initial cycle in the voltage range of 2.8-4.5 V.

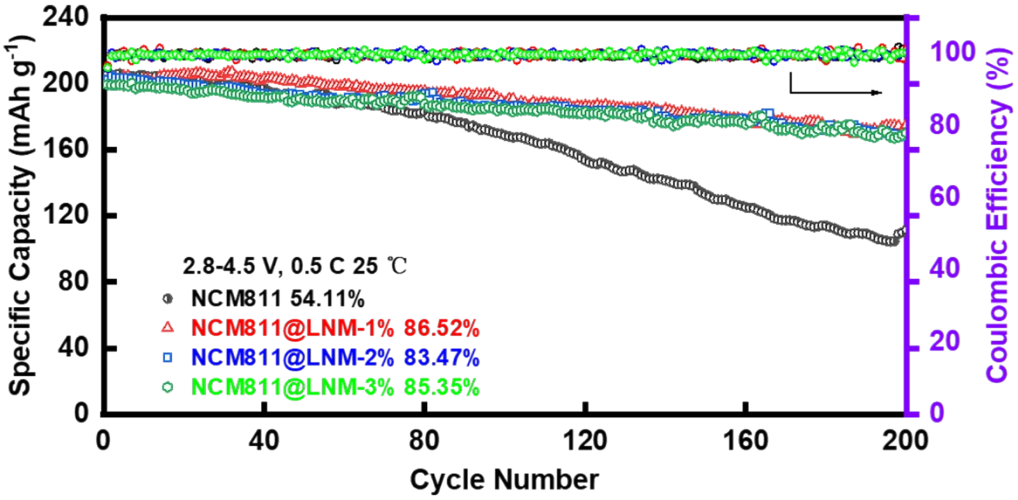


**Figure S9.** Cycling stability of NCM811, NCM811@LNM-1%, NCM811@LNM-2% and NCM811@LNM-3% against a lithium metal anode at 0.5 C from 1st to 200th under testing temperature of 25°C.

The NCM811@LNM-1% cathode material can deliver a satisfactory retention of 86.52% after 200 cycles, which are significantly higher than 54.11% retention of the bare NCM811 cathode. In addition, the NCM811@LNM-2% and NCM811@LNM-3% cathode material also can deliver a satisfactory retention of 83.47% and 85.35% after 200 cycles. So it can be seen that the LNM modification can greatly improve the cycle performance.

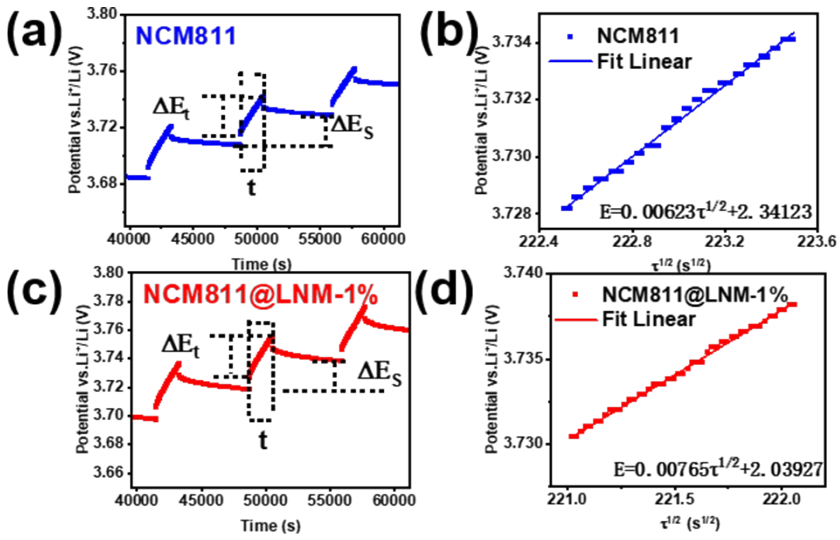


**Figure S10.** (a, c) Enlarged galvanostatic titration curves during charge and (b, d) the linear correlation between voltage change against $\tau^{1/2}$ for NCM811 and NCM811@LNM-1%, respectively.

The enlarged galvanostatic titration curves of NCM811 and NCM811@LNM-1% are shown in Figure S9. The linear correlation exists between voltage change against $\tau^{1/2}$ for NCM811 and NCM811@LNM-1%. The $Li^+$ ion diffusion coefficient ($D_{Li}$) can be determined according to the Fick's second law of diffusion. Based on the reasonable assumption that $\Delta E_\tau$ is linear with $\tau^{1/2}$, the formula can be simplified as:

$$D_{Li} = \frac{4}{\pi\tau}\left(\frac{mV_m}{MS}\right)^2\left(\frac{\Delta E_s}{\Delta E_\tau}\right)^2$$

where the values of $m$ and $M$ represent the mass and the molar mass of the active material, respectively. Besides, $S$ is the surface area of the electrode, $\tau$ is the constant current pulse time, $V_m$ is the molar volume of the active material, $\Delta E_s$ is the steady-state potential change and $\Delta E_\tau$ is the total potential change.[1, 2]

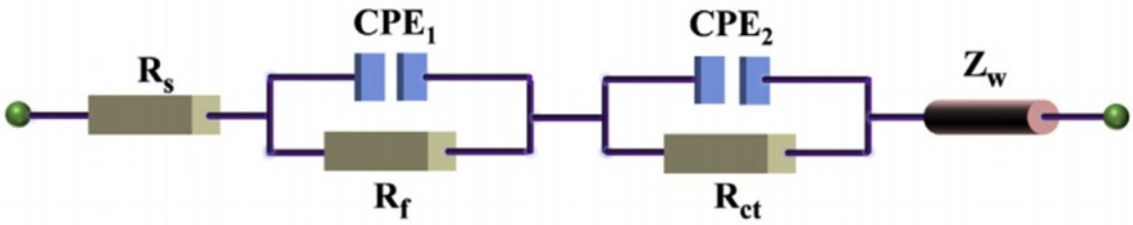


**Figure S11.** Simulated equivalent circuit based on the EIS measurements for NCM811 and NCM811@LNM.

In the fitted equivalent circuit, $R_s$ represents electrolyte resistance, $R_f$ corresponds to the semicircle at the highest frequency in the Nyquist plots which is related to the solid electrolyte interface (SEI) film resistance, $CPE_1$ is the correlated constant phase element, $R_{ct}$ corresponds to the second semicircle at high frequency, and $CPE_2$ represents the charge transfer resistance and correlated CPE, while $Z_W$ is Warburg impedance corresponding to the sloped line in the low frequency region which is related to solid-state diffusion of lithium ions in the electrode bulk.

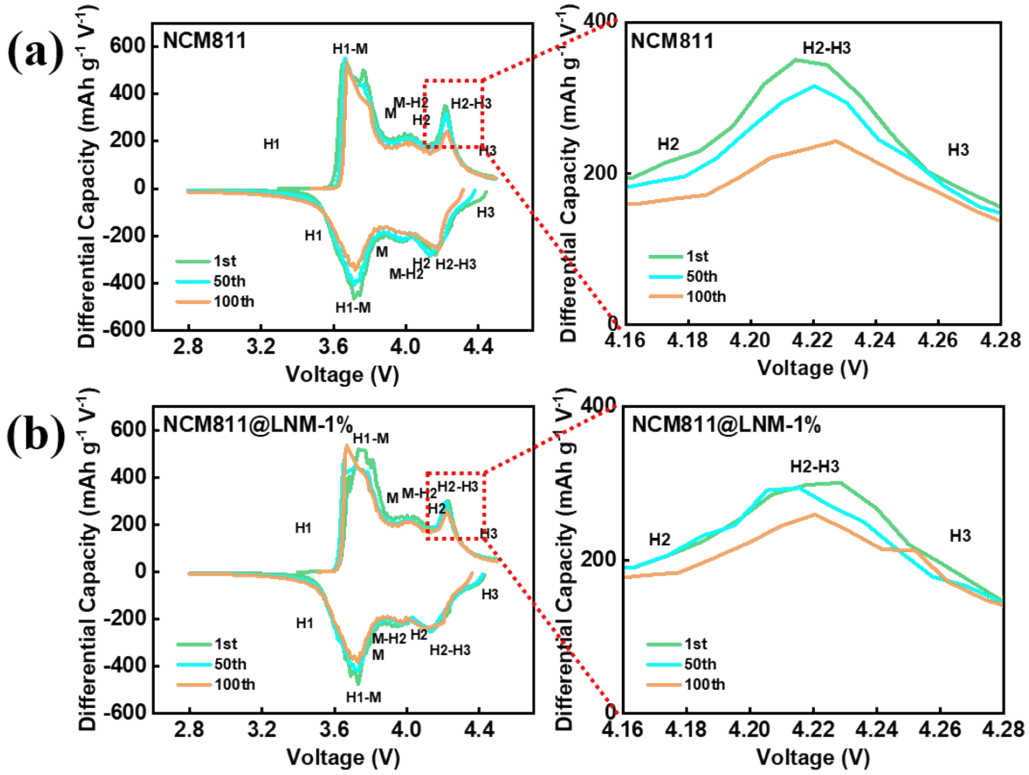


**Figure S12.** Corresponding dQ/dV curves of (a) pristine NCM811 and (b) NCM811@LNM-1% against Li metal anode from the 1st cycle to the 100th cycle.

The NCM811 and NCM811@LNM-1% cathodes undergo phase transformation during the delithiation, while the process happens reversibly during lithiation. It is reported that the H2 → H3 phase transition results in an abrupt unit cell lattice contraction along the c-direction. Thus the structure suffers from a severe mechanical strain with an anisotropic volume shrinkage under higher voltage. However, compared to the NCM811, a much higher reversibility across the H2-H3 phase transition is observed for the NCM811@LNM-1%, demonstrating the significantly alleviated degradation due to the conformal LNM modification.

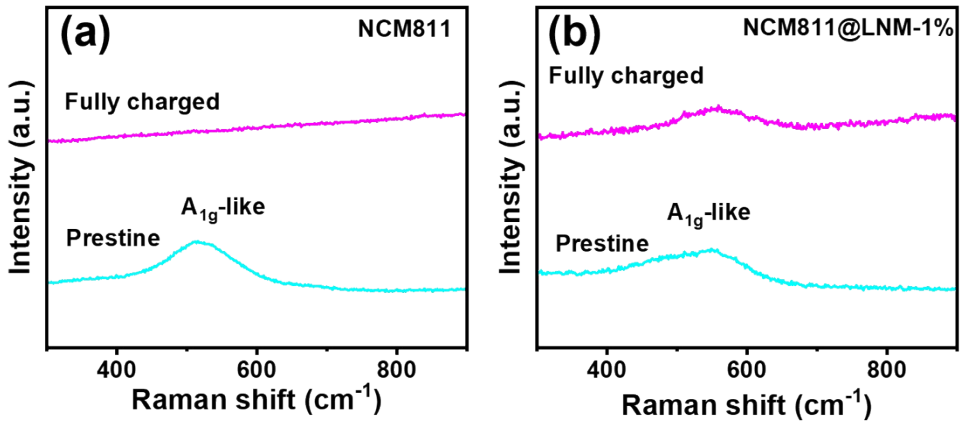


**Figure S13.** Ex situ Raman spectra of (a) NCM811 and (b) NCM811@LNM-1%.

In Raman spectra, the $A_{1g}$ mode represents longitudinal vibration of O in Ni-rich cathodes. Notably, the $A_{1g}$-like spectra decrease sharply during the process of full charge, and the obtained $Ni^{4+}$ can easily react with O to release oxygen, resulting in the lattice contracting abruptly and finally sharp reduction of the corresponding characteristic peaks. The results uncover that the extraction of $Li^{+}$ ion will lead to the instability of the original structure. The LNM modification can suppress oxygen release.

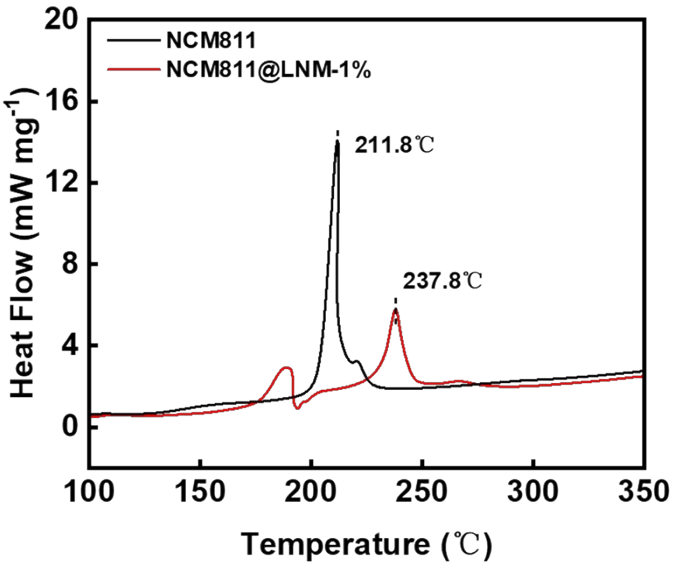


**Figure S14.** DSC curves of NCM811 and NCM811@LNM-1% after de-lithiation (charged to 4.5V).

Differential scanning calorimetry (DSC) measurement was applied to evaluate the stability of the materials at high temperatures. The exothermic peak for the charged NCM811 material emerges at 211.8°C, while the exothermic peak for the NCM811@LNM-1% rises to 237.8°C. These results indicate that the coating of LNM is beneficial to increasing the thermal stability of Ni-rich cathodes. Previous studies show that the highly charged Ni-rich cathodes would experience the phase transitions from a layered structure to a spinel structure and finally to a rock-salt structure upon heating, which is accompanied by the release of oxygen. [3-7] Obviously, better thermal stability implys that the LNM coating modification can suppress the evolution of $O_2$ gases from the active NCM811 core under higher temperature.

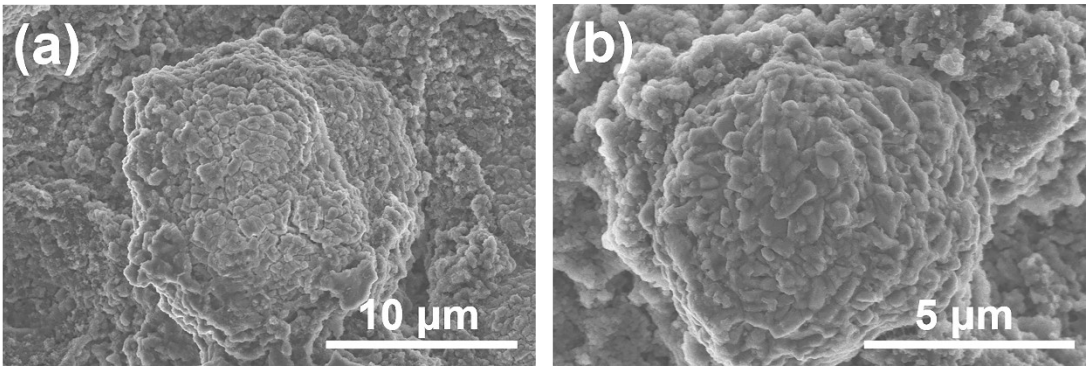


**Figure S15.** SEM images of (a) NCM811 and (b) NCM811@LNM-1% electrodes after 100 cycles.

The secondary particles of NCM811 electrode were severely cracked after 100 cycles. The NCM811@LNM-1% electrode maintains good integrity of secondary particles after 100 cycles due to the tight connection of primary particles by LNM modification, which alleviates the interfacial reaction with the electrolyte under high voltage.

**Table S1.** Experimental molar ratios of Ni: Co: Mn in NCM811. The experimental ratios were obtained by inductively coupled plasma mass spectrometry.

| Samples | mol / (%) |
|---|---|
| Ni/(Ni+Co+Mn) | 80.46 |
| Co/(Ni+Co+Mn) | 9.74 |
| Mn/(Ni+Co+Mn) | 9.79 |

**Table S2.** Structural information of NCM811, NCM811@$LiNi_{0.25}Mn_{0.75}O_2$-1%, NCM811@$LiNi_{0.25}Mn_{0.75}O_2$-2% and NCM811@$LiNi_{0.25}Mn_{0.75}O_2$-3%.

| Samples | a(Å) | c(Å) | c/a | (003) / (104) |
|---|---|---|---|---|
| NCM811 | 2.872 | 14.209 | 4.948 | 1.708 |
| NCM811@$LiNi_{0.25}Mn_{0.75}O_2$-1% | 2.870 | 14.216 | 4.952 | 1.777 |
| NCM811@$LiNi_{0.25}Mn_{0.75}O_2$-2% | 2.870 | 14.212 | 4.952 | 1.928 |
| NCM811@$LiNi_{0.25}Mn_{0.75}O_2$-3% | 2.872 | 14.219 | 4.952 | 1.879 |

**Table S3.** Particle size distribution of NCM811 precursor, NCM811 and NCM811@$LiNi_{0.25}Mn_{0.75}O_2$-1%.

| Samples | Size Distribution | $\mu m^{-1}$ |
|---|---|---|
| Precursor | D10 | 7.66 |
| | D50 | 11.69 |
| | D90 | 18.26 |
| NCM811 | D10 | 7.94 |
| | D50 | 14.75 |
| | D90 | 27.41 |
| NCM811@$LiNi_{0.25}Mn_{0.75}O_2$-1% | D10 | 6.85 |
| | D50 | 14.64 |
| | D90 | 33.39 |

**Table S4.** Cycling performances for different LNM modified NCM811 electrodes.

| Samples | Initial Discharge Capacity / (mAh $g^{-1}$) | Capacity Retention (after 200 cycles) / (%) |
|---|---|---|
| NCM811 | 205.8 | 54.11 |
| NCM811@LNM-1% | 202.4 | 86.52 |
| NCM811@LNM-2% | 202.7 | 83.47 |
| NCM811@LNM-3% | 199.3 | 85.35 |

**Table S5.** Comparison of cycling stability with the reported results in related literatures.

| Materials | Current Rate | Specific Capacity / (mAh $g^{-1}$) | Cycle Numbers | Operating Voltage / V | Capacity Retention / (%) | Ref. |
|---|---|---|---|---|---|---|
| NCM811@LNM-1% | 0.5 C | 202.4 | 200 | 2.8-4.5 | 86.52 | This work |
| 1%LYTP@SC-NCM88 | 0.5 C | 202.3 | 200 | 2.75-4.4 | 86.50 | [8] |
| NCM811@LMO-3% | 0.1 C | 201 | 100 | 2.7-4.3 | 92.9 | [9] |
| MP-NCM | 0.5 C | 191.4 | 100 | 3.0-4.3 | 86.3 | [10] |
| FC-NCM811 | 1 C | 182 | 300 | 2.8-4.5 | 84.3 | [11] |
| SC-NCM@LSTP-1% | 1 C | 170 | 400 | 2.75-4.6 | 77.4 | [12] |

**References**


1. K. M. Shaju, G. V. Subba Rao and B. V. R. Chowdari, *J. Mater. Chem.*, 2003, **13**, 106-113.
2. H. Zhang, Y. Liu, H. Jiang, Z. Deng, H. Liu and C. Li, *Chem. Eng. Sci.*, 2019, **207**, 611-618.
3. W.-S. Yoon, K. Y. Chung, M. Balasubramanian, J. Hanson, J. McBreen and X.-Q. Yang, *J. Power Sources*, 2006, **163**, 219-222.
4. Z. Cui, Q. Xie and A. Manthiram, *ACS Appl. Mater. Interfaces*, 2021, **13**, 15324-15332.
5. S.-M. Bak, K.-W. Nam, W. Chang, X. Yu, E. Hu, S. Hwang, E. A. Stach, K.-B. Kim, K. Y. Chung and X.-Q. Yang, *Chem. Mater.*, 2013, **25**, 337-351.
6. S. M. Bak, E. Hu, Y. Zhou, X. Yu, S. D. Senanayake, S. J. Cho, K. B. Kim, K. Y. Chung, X. Q. Yang and K. W. Nam, *ACS Appl. Mater. Interfaces*, 2014, **6**, 22594-22601.
7. L. Wang, T. Maxisch and G. Ceder, *Chem. Mater.*, 2007, **19**, 543-552.
8. X. Fan, X. Ou, W. Zhao, Y. Liu, B. Zhang, J. Zhang, L. Zou, L. Seidl, Y. Li, G. Hu, C. Battaglia and Y. Yang, *Nat. Commun.*, 2021, **12**, 5320.
9. X. Huang, W. Zhu, J. Yao, L. Bu, X. Li, K. Tian, H. Lu, C. Quan, S. Xu, K. Xu, Z. Jiang, X. Zhang, L. Gao and J. Zhao, *J. Mater. Chem. A*, 2020, **8**, 17429-17441.
10. D.-Y. Hwang, H.-S. Kim and S.-H. Lee, *J. Mater. Chem. A*, 2022, **10**, 16555-16569.
11. L. Zhang, S. Wang, L. Zhu, L. He, S. He, X. Qin, C. Zhao, F. Kang and B. Li, *Nano Energy*, 2022, **97**, 107119.
12. X. M. Fan, Y. D. Huang, H. X. Wei, L. B. Tang, Z. J. He, C. Yan, J. Mao, K. H. Dai and J. C. Zheng, *Adv. Funct. Mater.*, 2021, **32**, 2109421.